Graded open-cell aluminium foam core sandwich beams

Arnaud Pollien [a], Yves Conde [a], Laurent Pambaguian [b], Andreas Mortensen [a],*

[a] *Ecole Polytechnique Fédérale de Lausanne (EPFL), Laboratory for Mechanical Metallurgy,*
Institut Des Matériaux, Station 12, MX-D141, CH-1015 Lausanne, Switzerland
[b] *European Space Agency ESA-ESTEC, Material Mechanics and Processes Section, Keplerlaan 1,*
P.O. Box 299, NL-2200 AG Noordwijk ZH, The Netherlands

Abstract

We show that the replication process can be extended towards the production of functionally graded porous structures by fabricating and testing structures in which outer layers of dense metal encase a central part made of foam with graded porosity. Samples of this kind are produced by pressing individual layers of NaCl powder of granulometry 60–90 μm, and then stacking these layers between two skins of dense aluminium. The stacked preforms are then infiltrated with pure aluminium and solidified before dissolution of the salt in water. Specimens containing up to five layers of porous Al of different density between two dense outer skins of pure Al are produced; selected samples are tested in three-point bending. Data show good agreement with analysis based on sandwich beam theory and the Deshpande–Fleck yield criterion. Results of this work indicate that whereas lightweight graded metal/metal foam beams show little promise from the standpoint of stiffness-limited design, they may be of interest from the standpoint of load-limited design.
© 2005 Elsevier B.V. All rights reserved.

Keywords: Aluminium; Foam; Replication; Sandwich; Bending; Yield

1. Introduction

There is currently much interest in metal foams in large part because such materials are now commercially available [1–5]. Target structural applications include components for mechanical energy absorption [6–8] and more generally light-weight structural elements, such as sandwich structures where two thin outer «skin» layers of a dense stiff material are separated by a central «core» of foamed metal. Aluminium skin/aluminium foam sandwich structures have thus been the subject of a considerable body of recent research [2,9–19], as have other dense metal/metal foam structures, such as cylindrical shells and foam-filled metal tubes [2,3,5,7].

To produce such structures, two routes can be used; either they are produced in one processing step from the same metal (e.g., [20–22]), or alternatively the dense metal and the foam are separately produced and then bonded together. The dense metal and metal foam are bonded either with an organic adhesive (e.g., [10,14,17]) or by casting the metal around the foam (e.g., [23,24]). With the exception of work recently reported in Ref. [21], closed-pore foam cores of homogeneous density have always been used in sandwich beams tested for mechanical properties [13,17,25–27].

Porous materials are frequent in nature; wood and bone are well-known examples. Often, these natural porous structures are graded, meaning that the porosity is not uniform. Rather, it is distributed in space so as to maximize the overall performance of the structure; an example is provided by bone, in which regions of dense "cortical" bone neighbour regions of lower-density "trabecular" bone, the solid density being distributed in space so as to optimise the mechanical performance of the overall bone structure [28]. In other words, bones are "functionally graded material structures" [29].

It may, therefore, be of interest to produce such graded structures in metal foam as well [28]. This was attempted in Ref. [21], with magnesium structures made of two concentric cylinders having different pore sizes encased in a dense layer of metal and produced by infiltration of NaCl preforms. The attempt unfortunately proved unsuccessful because the

---

* Corresponding author. Tel.: +41 21 693 29 12; fax: +41 21 693 46 64.
E-mail address: Andreas.Mortensen@epfl.ch (A. Mortensen).

magnesium was heavily corroded during leaching of the salt in water.

We show in this paper that the replication process can indeed be extended towards the production of graded porous metal structures by producing and testing sandwich structures in which outer layers of dense aluminium encase a central part made of aluminium foam, which itself features spatial variations in foam porosity across the beam thickness. These samples are also tested in three-point bending and test data are compared with predictions based on engineering beam theory.

2. Experimental procedures

2.1. Processing

The replication process as applied to the production of porous aluminium is described in Refs. [30–33]. It comprises four essential steps, namely: (i) preparation of a preform of compacted NaCl powder; (ii) infiltration of the preform with molten aluminium; (iii) solidification of the metal; (iv) dissolution of the salt in water. The resulting open-pore aluminium foam (or "sponge") features open porosity, the scale and volume fraction of which can be controlled by tailoring the size and packing density of the salt used to make the preform.

Salt preforms of this work were produced using commercial purity NaCl powder (CP1 salt and >98% NaCl with 1–2% $Ca(PO_4)_2$ anticaking agent) purchased from Salines de Bex (Bex, Switzerland). The powder was first sieved, retaining powder particles in the size range 63–90 μm. It was then pressed into flat homogeneous layers using a die and two mobile punches mounted on an electromechanical testing machine. With this technique, by varying the applied pressure, the volumic fraction of salt can be varied between 0.55 and 0.85, corresponding to aluminium volume fractions of 0.45 and 0.15, respectively. In this specific investigation, the salt volume fraction was chosen within a tighter range because: (i) long beams 1 mm thick of pressed NaCl powder having a volume fraction below 0.60 are too weak to be handled and (ii) volume fractions above 0.75 required a load exceeding the press capacity. The foam relative density was thus varied between 25 and 40% (i.e., the salt volume fraction was between 75 and 60%). In pressing each layer, the parallelism of both punches was controlled such that their separation was constant within 0.01 mm along the 150 mm length of the sample.

For the production of structures in which two uniform layers of dense metal encase a central core of foam with graded foam porosity, salt preforms were made by stacking discrete salt layers of different density. A pressed and assembled preform is shown in Fig. 1. It comprises five salt layers, encased between two solid aluminium layers, each 2 mm thick (temporarily held together with masking tape).

One or two such assembled salt and aluminium sheet preforms were inserted into a crucible of dense alumina 35 mm
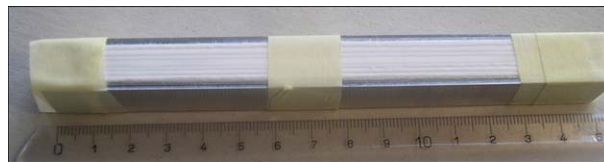

Fig. 1. A preform consisting of a stack of salt layers and aluminium sheets.

in diameter. A cast cylindrical ingot of high-purity (99.99%) aluminium was placed in the crucible on top of the preform before infiltration. The empty space around the preforms in the crucible was filled with a fine (5 μm) alumina powder. This powder was selected because it is not infiltrated with aluminium at the infiltration pressure used; hence, it remained a loose powder, easing extraction of the sample from the crucible after infiltration.

The crucible containing the packed preform and metal was inserted into a custom-built infiltration apparatus, which was then evacuated using a rotary pump to 2–3 Pa residual gas pressure. The temperature was raised to 710 °C, to melt the aluminium ingot and sheets along the salt preforms. After a 1 h hold at 710 °C, argon gas pressurized at 0.65 MPa was let into the infiltration chamber, forcing the molten metal into the salt preform. After infiltration, the crucible was lowered onto a copper chill, heating was discontinued and the infiltrated aluminium was solidified directionally along the axis of the crucible from bottom to top.

Machining was performed at this stage, to bring the outer skin thicknesses to their target value of 1 mm. Machining was also used to compensate slight deformation of the casting or slight misalignments of individual layers therein. To remove the salt, the sample was finally immersed for 30 h in cold distilled water, changing the water every hour during the first 10 h.

The overall beam geometry was designed to fit requirements for flexural testing according to ASTM C393; in particular, this requires a rectangular cross-section and a sample width no less than twice its total thickness. Rectangular beams were thus produced, with target width, height and length at 20, 10 and 150 mm, respectively.

2.2. Mechanical testing

Three-point bend tests were performed at room temperature at a cross-head speed of 1 mm/min on a MTS Alliance RT/50 electromechanical testing machine. The diameter of the rollers was 5 mm; these were applied directly on the samples. The total span length between the lower rollers was 95 mm in all tests and the imposed mid-point movement rate was 1 mm/min. During the test, digital pictures of the beams were taken at various load values, to aid identification of failure modes.

Two further tests were performed:

(i) One with a rigid steel beam replacing the test sample. This was used to measure the overall machine

compliance, which was needed to calculate the sample deflection.

(ii) One with the same rigid steel beam together with annealed aluminium skins placed between the rollers and the steel beam. This second set-up replicated the combined effects of machine compliance and indentation of the skins by the rollers. It was found that the additional deflection due to the skins ceases to increase at a load of 3 N/mm. Hence, at linear load values above 3 N/mm the data are free of artefacts caused by indentation of the soft aluminium sample outer skins by the rollers. As will be seen below, at 3 N/mm, the samples still deform elastically.

3. Experimental results

3.1. Macrostructural characterization

Seven graded porosity beams were tested; Table 1 gives their main geometrical and structural characteristics. The average skin thickness was calculated by subtraction of the total core thickness from the beam thickness. The core thickness was calculated by addition of the thickness of the single salt layers (these were found to be unchanged after infiltration). Specifics of this calculation are given in Table 1. One additional sample, containing five layers in its porous core, was also produced but not tested.

For the specimens reported in Table 1, the skin thickness was also optically measured during and after machining. It was kept within ±0.1 mm of the 1 mm target value. Maintaining precise parallelism between the foam layers on one hand and between the skins and the foam layers on the other hand, proved challenging, slight movements or deformation of preform elements during handling, heating or infiltration causing significant error. Samples with parallelism errors greater than 0.2 mm over the total sample length of 150 mm were rejected. Those for which parallelism errors were less than 0.2 mm were further processed, using machining to achieve an even outer skin thickness. Overall, final dimensions of the samples are generally within the target geometry requirement. The only accepted exception was when width and/or length
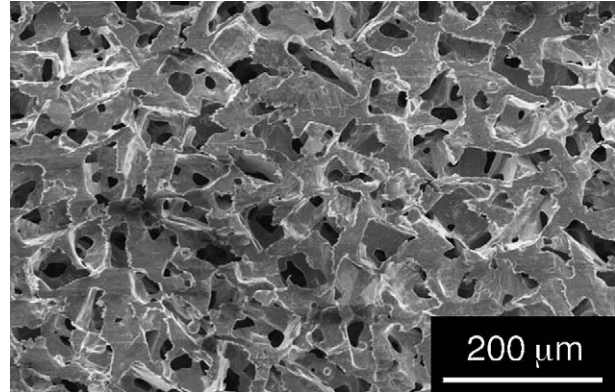

Fig. 2. SEM micrograph of the machined surface of 63–90 foam of relative density (i.e., aluminium volume fraction) 30.5%.
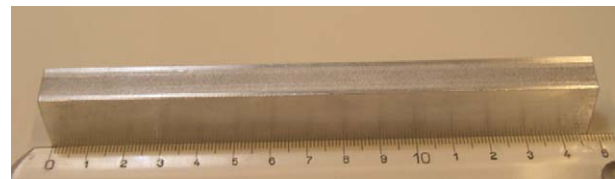

Fig. 3. General view of a seven-layered beam (Sample B1, comprising of two dense skins and five foam layers of differing density).

were slightly lower than targeted because a few imperfections along the outer faces were removed by machining.

3.2. Microstructural characterization

Fig. 2 shows a scanning electron micrograph of a polished surface of aluminium foam produced using 63–90 μm salt. The microstructure is homogeneous, featuring aluminium nodes and struts surrounding angular pores having a shape "replicating" that of the salt powder used to produce the preform.

A general view of the five-layered beam is shown in Fig. 3. A more detailed view of the different layers of the same beam is shown in Fig. 4. An interface between two layers of foam with different porosity is shown at higher magnification in Fig. 5. No discontinuity or evidence of a weak layer can be observed in such interfacial regions between foam layers;

Table 1
Description of the fully processed samples

No.	Structure[a]	Overall dimensions				Skins[b]	Outer layer		Center layer		Outer layer	
		m [g]	h [mm]	b [mm]	L [mm]	t [mm]	V_{f_2}	c_2 [mm]	V_{f_1}	c_1 [mm]	V'_{f_2}	c'_2 [mm]
A1	1L1	33.5	10.86	18.50	147.6	0.93	–	–	0.263	9.00	–	–
A2	1L1	33.1	11.00	17.89	147.6	0.99	–	–	0.265	9.02	–	–
A3	1DLD1	36.5	11.26	18.30	146.3	1.14	0.382	2.48	0.250	4.03	0.375	2.47
A4	1DLD1	38.9	11.14	17.46	145.9	1.07	0.373	2.45	0.257	4.09	0.377	2.47
A5	1LDL1	33.8	11.10	17.92	145.9	1.01	0.259	2.59	0.385	4.02	0.254	2.48
A6	1D1	41.5	11.33	17.90	148.1	1.12	–	–	0.380	9.10	–	–
A7	1D1	40.9	10.96	17.80	147.6	0.95	–	–	0.380	9.07	–	–

[a] Stacking from one outer skin to the other. Dense Al skins are represented by "1", The denser foam layers are noted "D" and the lighter ones are noted "L".
[b] Average thickness of one skin: $t = 0.5 \times (h - (c_2 + c_1 + c'_2))$.
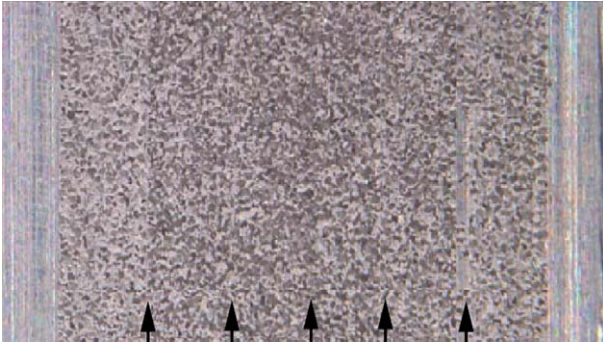
Fig. 4. Transverse cross-section of the seven-layered beam of Fig. 3. The dense aluminium skins are at the left and right of the picture. In between, five (vertical) individual layers of foam can be observed; layer transitions are arrowed. The dense outer skins are 1 mm thick, which sets the scale of the picture.

on occasion a thin layer of dense aluminium fills gaps left between the preform layers.

The interfaces between the foam and the dense aluminium skins present slight microstructural imperfections caused by the oxide layer covering the solid metal skins before infiltration. Therefore, the bond between the foam core and the outer dense metal layer was somewhat weaker than would be a purely metallurgical transition from dense to porous metal. As will be seen below, the poor resistance of the dense to porous metal interface becomes apparent when samples fail towards the end of bend testing; however, in as-infiltrated samples and in initial stages of bend testing, the resulting interfacial bond strength proved sufficient.

3.3. Mechanical characterization

Three-point bend testing was performed on seven symmetrical samples that were roughly within 10% of the target sample geometry (Table 1). The core was composed of a
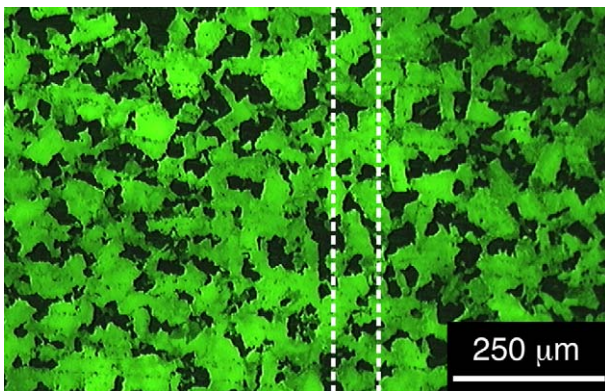

Fig. 5. Optical micrograph of interfacial regions separating discrete porous metal layers. The foam was infiltrated with a fluorescent resin such that aluminium appears black while the resin, which shows the pore space in the foam, appears green (light grey in black and white). The interface is located between the dotted lines. "For interpretation of the references to color in this figure legend, the reader is referred to the web version of the article."
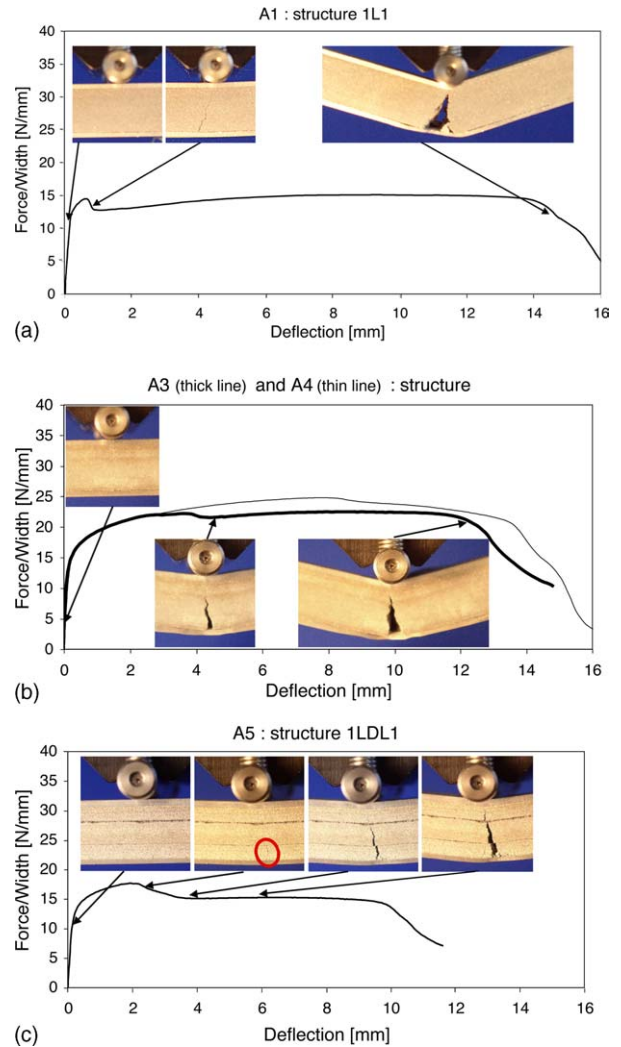

Fig. 6. Load–deflection curves and localisation of rupture: (a) structure 1L1; (b) structure 1DLD1; (c) structure 1LDL1.

symmetrical stacking of one or both of the two extreme foam densities achievable with the present processing route (roughly 25 and 40 vol.%).

Results for selected beams are given in Fig. 6, while Fig. 7 collects all load/displacement curves for this test series. To
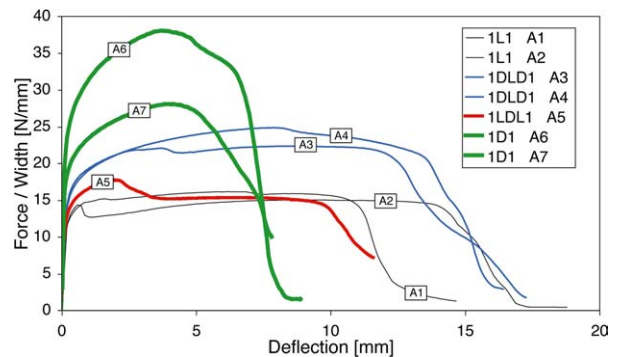

Fig. 7. Linear force–displacement diagrams for seven samples of same geometry tested in three-point bending (span length = 95 mm).

enable the direct comparison of results, the force values have been normalised by dividing the recorded load by the individual beam width. Pictures of the beams under the central point are superimposed over the plots showing failure mechanisms. The data show that:

(i) All samples display a linear regime of deformation after the short initial transient corresponding to setting-in of the rollers by indentation of the skins (see Section 2.2 above). It was ascertained with a separate test that this deformation corresponds to linear elastic deformation of the beam; deformation in this region is linear reversible and after the onset of plastic beam, the unloading modulus of the sample is unaffected. The present samples thus do not display the difference in loading and unloading modulus that is often reported for sandwich structures made with commercial closed-cell foams [16,19].

(ii) At higher stresses, the load–displacement curve deviates from linearity, displaying a permanent deformation after unloading; plastic yielding begins. The yield stress was defined as the flow stress at a plastic offset deflection of 20 μm (this value was arbitrarily chosen as a small yet detectable offset).

(iii) The flow curve is dependent on the foam core structure, increasing with increasing average foam density in the core (Figs. 6 and 7); however, the flow curve is also dependent on the skin thickness, as can be seen by comparing the two curves in Fig. 7 for the 1D1 structures, noting that there is a 20% difference in outer skin thicknesses between the two (1.12 mm versus 0.95 mm).

(iv) In all samples, the first sign of visible damage appeared well beyond yield and consisted in the nucleation and growth of one or two cracks within the core, located along the sample length slightly off but near the middle (i.e., nearly, under the central load line). As they developed, these cracks were slightly inclined with respect to the load axis, pointing towards the load application line (see photographs in Fig. 6).

(v) Once these cracks had nucleated, the load–displacement curve became less regular, the load at times decreasing with increasing deformation.

(vi) Upon further deformation of the sample well past the point of crack nucleation, cracking progressed with the bottom metal skin deforming in localized tension under the top roller (Fig. 6). Final failure and unloading was caused by tensile failure of the lower aluminium skin.

4. Discussion

4.1. Elastic deformation: beam flexural rigidity

The geometry of beams tested in three-point bending is sketched in Fig. 8. The core has up to three layers, the central layer having a relative density V_{f_1} and a thickness $c_1 = 2h_1$, while the external layers both have relative density V_{f_2} and
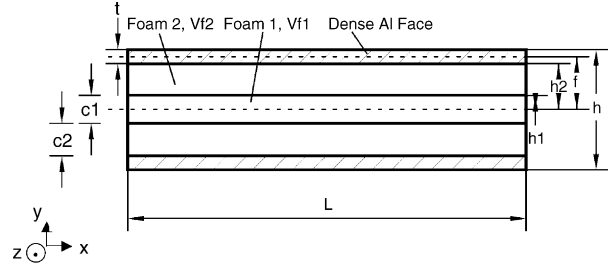

Fig. 8. Sandwich beam with a graded core (three layers), described with six parameters: V_{f_1}, V_{f_2}, h_1, h_2, h and m.

thickness $c_2 = h_2 - h_1$. The total height of the beam is denoted as h, while b and L are the beam width and length. The two outer dense aluminium faces have a fixed thickness t. The total core thickness of such a beam is then $2h_2 = h - 2t$ and the distance between the centroid of the beam and that of the dense outer skins is $f = (h - t)/2$ (Fig. 8). The flexural rigidity D of the sandwich beam defined in Fig. 8 is the sum of the flexural rigidities of the faces and the core [9]:

$$D = D_f + D_{c_2} + D_{c_1} = \left(\frac{E_f b t^3}{6} + 2E_f t b f^2 \right)$$

$$+ \left(\frac{E_2 b c_2^3}{6} + 2E_2 c_2 b \left(\frac{c_1 + c_2}{2} \right)^2 \right) + \left(\frac{E_1 b c_1^3}{12} \right) \tag{1}$$

where E_f is the Young's modulus of aluminium and E_i denotes the Young's modulus of the aluminium foam in layer i, given for the foams of this work by Refs. [33,34]:

$$E_i = 33 V_i^2 \ (\text{GPa}). \tag{2}$$

If:

$$12 \left(\frac{f}{t} \right)^2 \geq 100$$

$$12 \frac{E_f}{E_2} \left(\frac{f^2 t}{c_2^3} \right) \geq 100,$$

$$\frac{E_f}{E_2} \left(\frac{f^2 t}{\left(\frac{c_1 + c_2}{2} \right)^2 c_2} \right)^2 \geq 100,$$

and

$$12 \frac{E_f}{E_1} \left(\frac{f^2 t}{c_1^3} \right) \geq 100$$

then Eq. (1) reduces to [1]:

$$D = 2E_f t b f^2 \tag{3}$$

The four above conditions are obeyed in nearly all configurations considered here. The core thus exerts little influence on the stiffness of these beams in pure bending; however, in

the calculations given below, the full expression Eq. (1) was nonetheless used.

In three-point bending, the rigidity of a sandwich beam, defined as the ratio of the load P to the deflection in the elastic domain δ, is given by Ref. [35]:

$$\frac{P}{\delta} = \frac{1}{\left(\frac{L^3}{48D}\right) + \left(\frac{L}{4AG}\right)} \tag{4}$$

where D is the flexural rigidity of the beam (given by Eq. (1)), A the cross-sectional area of the beam core and G is the average in-plane shear modulus of the core [2,35].

The expected rigidities of Samples A2–A7, as calculated using Eq. (4) (computing G of the foams as $E/2(1 + \nu)$, where E is Young's modulus and $\nu = 0.33$ is the Poisson ratio) are compared with the measured rigidities (corrected for machine compliance) in Table 2. Sample A1 was not compared because there were too few data points in the linear elastic regime of deformation.

Measured values are between 60 and 98% of the predicted values. The agreement is deemed satisfactory given uncertainty in experimental data (similarly, discrepancies of up to 20% were found in Ref. [36]). Discrepancies can have several sources:

(i) Uncertainty in the skin thickness, estimated to be on the order of 10% ($\pm 100\,\mu$m) along the length of the beam, will induce an uncertainty on the order of 10% on D (see Eq. (3)). Since the rigidity of these beams is only partly determined by their flexural rigidity (because of the significant contribution of core shear), this may explain some, but not all, of the discrepancy.

(ii) There may be additional modes of deformation of the beams, over and above what is predicted by simple beam theory. Specifically, there may be some additional elastic deformation of the beam along the vertical direction. By inserting the end of a tested beam between the central roller and the steel beam used for compliance calibration of the testing apparatus, it was noticed that a higher compliance is recorded. There was obviously no bending of the sandwich beam in this configuration; the added elastic strain was caused by foam deformation under the roller in indentation mode. The presence of such added deformation would, indeed, account for the fact that the largest discrepancy between predictions

from beam theory and experimental data are for those beams with a layer of low-density foam and are highest for the beam with a core fully composed of this material (A2).

Overall, the results show that the stiffer beams are those with the highest volume fraction of metal in their core; this clearly stands to reason given the fact that sample dimensions were kept constant. From the standpoint of structural optimisation for lightweight construction, the conclusion is of course different, since it is then sought to maximize the beam stiffness at constant mass. Analysis based on equations above then shows that optimal performance is obtained with a uniform core of the lowest density foam (this is illustrated in Appendix A). From the standpoint of specific stiffness, graded porosity core beams thus seem to be of little practical interest.

4.2. Failure by yielding

We now consider the onset of yielding in single and three-layered beams manufactured in the frame of this study. This is interesting for two reasons:

(i) From a practical standpoint, the onset of plastic deformation is often taken to define the maximum load that can be borne by a structural material before it is considered to have failed.

(ii) From the standpoint of yield, there is a motivation to explore graded beams. Indeed, yielding of metal/metal foam beams in bending with a gradient in the applied moment (something which is encountered in nearly all practical situations, including three- and four-point bend testing), is dictated by a combination of tensile and shear stresses, both of roughly equal magnitude in a foamed metal core [14]. The relatively strong variations in the combination of these stresses across the thickness of the beam (the elastic tensile stress increasing linearly with increasing distance from the neutral axis and the shear stress increasing far more slowly but in the opposite direction) may motivate the creation of gradients in foam density so as to delay, for a constant beam mass and geometry, the moment when yield occurs within the core, or so as to minimize the beam mass for a given design load.

For the beam configuration of Fig. 8, in linear elastic deformation the normal stress in the ith layer of the sandwich beam, $\sigma_{x,i}$, is linearly related to the applied moment M knowing the Young's modulus of the considered layer E_i, the local flexural rigidity of the beam D (Eq. (1)) and height y referenced to the central axis (Eq. (5)):

$$\sigma_{x,i} = \frac{ME_i}{D}y \tag{5}$$

The axial tensile stress profile along the y-direction is thus discontinuous across the interfaces between the layers made of different materials.

Table 2
Calculated and measured rigidities P/δ

NR	Calculated P/δ [N/mm]	Measured P/δ [N/mm]	Δ [%]
A2	2418	1471	−40
A3	2366	1840	−23
A4	2209	1671	−25
A5	2151	1418	−35
A6	3350	2695	−20
A7	2869	2828	−2

The shear stress profile in a rectangular sandwich beam along the y-direction, τ, is [2, p. 11]:

$$\tau = \frac{Q}{bD}\sum_i (SE)_i \tag{6}$$

where Q is the shear force at the section, equal to the local rate of variation of the moment with distance along the beam length: $Q = dM/dx$, D the flexural rigidity of the entire section, Σ stands for summation over i where i identifies each layer of the beam, b the width of the beam and S is the first moment of area of the cross-section in each layer above the y-coordinate at which τ is being evaluated:

$$S = b \int y \, dy. \tag{7}$$

As demonstrated in Ref. [14], the state of stress is multiaxial in the aluminium foam core of such a sandwich beam:

$$\underline{\sigma} = \begin{pmatrix} \sigma_c & \tau_c & 0 \\ \tau_c & 0 & 0 \\ 0 & 0 & \upsilon\sigma_c \end{pmatrix} \tag{8}$$

where σ_c and τ_c are the normal and shear stresses in the core, defined, respectively, in Eqs. (5) and (6) and $\underline{\sigma}$ is the stress tensor. The coefficient υ allows to adjust the stress in the z-direction between plane strain (in which case $\upsilon = \nu$, the

core material Poisson's ratio taken to equal 0.33 in calculations) and plane stress (in which case $\upsilon = 0$); the latter case is assumed in calculations, since failure was observed at the sample surface.

Since the stress state can be multiaxial in a sandwich core, a multiaxial yield criterion is needed. We use the criterion proposed by Deshpande and Fleck [37]:

$$\frac{1}{1 + \left(\frac{\beta}{3}\right)^3}\left[\left(\frac{\sigma_e}{\sigma_y}\right)^2 + \beta^2\left(\frac{\sigma_m}{\sigma_y}\right)^2\right] = 1 \tag{9}$$

where σ_m and σ_e are the mean and von Mises equivalent stresses, respectively. The constant β in Eq. (9) is related to the compressibility of the foam; the exact value of β is not known for the type of open-cell foams used here. We therefore estimate β by taking the reported value for another open-cell aluminium, namely the Duocel foam: $\beta = 1.58$ [37].

Consider now the beam defined in Fig. 8 subjected to three-point bending. There are two points at which core yielding may start:
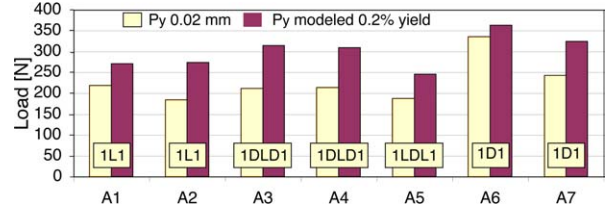

Fig. 9. Predicted and measured yield loads of the seven beams given in the first series of Table 1; experimental data are from Fig. 7.

(i) at the interface between Layers 1 and 2 ($y = h_1$);
(ii) at the interface between Layer 2 and the skin ($y = h_2$),

in both cases right under the central applied load (at $x = L/2$), where the maximum moment M and shear force Q (at $x = L/2$) are, respectively:

$$M = \frac{PL}{4} \tag{10}$$

and

$$Q = \frac{P}{2}. \tag{11}$$

The stress state at theses two points is obtained by calculating σ_m and σ_e from Eq. (8) knowing σ_c and τ_c from Eqs. (5) and (6), respectively, at $y = h_1$ and h_2, for a beam of given E_i and D. Substitution into Eq. (9) then defines P_{y_1} and P_{y_2}, the loads at which yield occurs at $y = h_1$ and $y = h_2$, respectively:

$$P_{y_1} = 4\sigma_{y_1}bD\sqrt{\frac{9 + \beta^2}{108S_1^2 + b^2 E_1^2 h_1^2 L^2(\beta(1 + \upsilon)^2 + 9(1 + (\upsilon - 1))\upsilon)}} \tag{12}$$

$$P_{y_2} = 4\sigma_{y_2}bD\sqrt{\frac{9 + \beta^2}{108S_2^2 + b^2 E_1^2 f^2 L^2(\beta(1 + \upsilon)^2 + 9(1 + (\upsilon - 1))\upsilon)}} \tag{13}$$

where S_1 and S_2 are the first moments of areas above $y = h_1$ and $y = h_2$:

$$S_1 = \frac{E_f b}{2}\left(\frac{h^2}{4} - d^2\right) + \frac{E_2 b}{2}\left(d^2 - \frac{c_1^2}{4}\right) \tag{14}$$

$$S_2 = \frac{E_f b}{2}\left(\frac{h^2}{4} - d^2\right) \tag{15}$$

The limit load of the beam for the onset of yield in the core is the lower of P_{y_1} and P_{y_2}.

It is difficult to compare the predicted limit load with experimental data because in both experiments and in using the above expressions (Eqs. (12) and (13)), yield is defined using somewhat arbitrary offset deformations. Experimental $P(\delta)$ curves deviate very gradually from linear behaviour (Figs. 6 and 7). We have, therefore, taken a relatively arbitrary definition of yield as being the load «$P_{y = 0.02\,mm}$» at which the lowest accurately measurable permanent deflection of 20 μm is reached; these values are plotted in Fig. 9 as $P_{y = 0.02\,mm}$, measured on Samples A1–A7. Also, since the present aluminium foam materials themselves yield very gradually (they
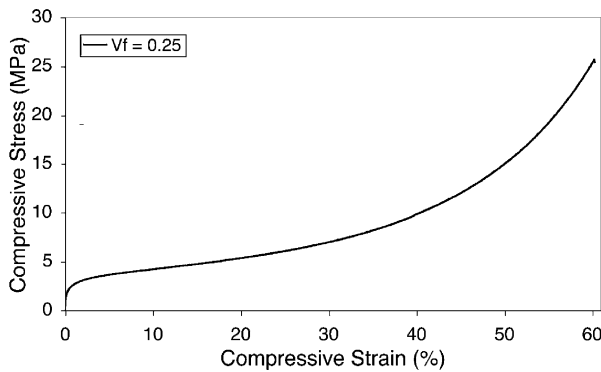
Fig. 10. A typical compression curve for the open-cell foams used as core materials in this study. The relative density of the foam is 0.25.

display the same power-law behaviour as the metal they are made from, see Fig. 10 and Ref. [33]), we have defined the foam yield stress as that which produces a uniaxial plastic strain of 0.2%. We used the relation measured in replicated pure Al foams having a cell size of 400 μm, which were extensively characterized in Ref. [33], corrected by a constant multiplicative factor for the observed foam hardening that comes as a result of a reduction of the average cell size from 400 to 75 μm, the average cell size in the present foams [34]. This gives the yield stress under uniaxial stress as a function of $V_{f,i}$, the foam relative density in layer i, as:

$$\sigma_{y,i} = 1.88 \times 36 \times (0.002)^{0.26} \times V_{f,i}^{1.63} = 13.45 V_{f,i}^{1.63}. \tag{16}$$

This yield stress is then used to compute beam yield loads given by Eqs. (12) and (13); the lower value is the predicted beam yield load, also given in Fig. 9. In the calculation, measured sample geometrical parameters given in Table 1 were used.

As illustrated in Fig. 9, the predictions overestimate by about 20% the experimental values; however, observed variations in the yield stress are relatively well predicted. In particular, the significant difference between the two 1D1 beams, Samples A6 and A7, is again explained by geometrical differences (Table 1). The systematic difference between prediction and experiment is not surprising, since the predicted and the experimental values of the yield load are, as mentioned in what precedes, both defined using arbitrary offset plastic deformations.

From the data, it emerges that the best performance in terms of yield load is achieved by the beams having the densest core (1D1; Samples A6 and A7). These are the most rigid beams (Table 2) but also the heaviest. To aid comparison, the curves in Figs. 6 and 7 were also normalised with respect to the beam mass per unit width. The ranking remains the same among beams tested here; those with the denser core are also those showing the best performance in terms of specific-load-bearing capacity past the onset of yield.

It is also interesting to note that the predicted location of first yielding is, for all beams tested, at the outermost y-value in the low-density layer. In LDL cores first yielding is predicted along the layer/skin interface, while in DLD cores first yielding is predicted in layer 1 at the L/D interface between core layers 1 and 2. This has the implication that from the standpoint of resistance to yield and hence, from the standpoint of specific-load-limited sandwich design in the beam and test geometries considered here, using the lightest foam is not optimal (as it was for elastic rigidity). From this standpoint, there may, thus, be a practical interest in graded metal foam core sandwich beams.

Following yield, deformation continues, leading to the nucleation and growth of a near-mode I crack under the central load application point for all the series of seven beams tested (Table 1). In these beams, the first failure mechanism is clearly by core shear. Upon continued deformation, damage then progresses by opening of the crack, delamination along the skin/foam interface aided by the weakly bonded oxide skin covering the dense Al layers and finally tensile tearing of the lower skin (see Fig. 6).

Finally, we would like to emphasize that the performance of these beams could be easily improved as pure aluminium, having a very low yield stress, was used for both the foam and the skins. This choice was motivated by the availability of data on their mechanical behaviour from earlier work on replicated pure aluminium foams; however, far better mechanical performance would obviously be obtained using an aluminium alloy [31,33,34].

5. Conclusion

(1) Complex metal/metal foam graded sandwich beams can be produced by replication processing. The capacity to manufacture graded beams containing up to five layers of controlled density and thickness between two dense outer skins of the metal making the foam is demonstrated.

(2) Metal/metal foam sandwich beams containing a core composed of one or three layers of metal foam were produced and tested in bending. Their behaviour was analyzed for elastic rigidity and resistance to plastic deformation. Data and analysis show overall good agreement.

(3) This study also indicates that whereas lightweight graded metal/metal foam beams show little promise from the standpoint of stiffness-limited design, they may be of interest from the standpoint of load-limited design.
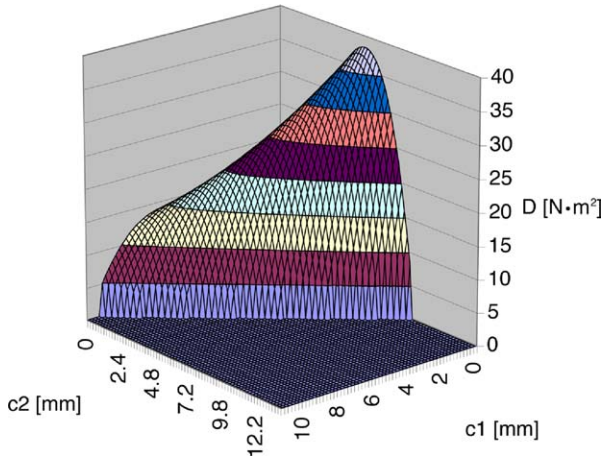
Acknowledgements

Fig. 11. Flexural rigidity of a graded beam as a function of the core layers thicknesses c_1 and c_2, for $m = 10\,\mathrm{kg/m^2}$.

Appendix A. Flexural rigidity of a symmetric sandwich beam containing a three-layered core

Fig. 11 shows a plot of the flexural rigidity D of the graded beam depicted in Fig. 8 calculated using Eq. (1) with relative densities V_{f_1} and V_{f_2} fixed at 0.35 and 0.2, respectively, a total beam mass held constant at $m = 10\,\mathrm{kg/m^2}$, plotted as a function of c_1 and c_2. Note that in the calculation, the outer skin thickness is a function of the thickness and density of core layers, since the total beam mass is constant (the core mass is determined by c_1 and c_2; the total beam mass then determines the thickness of the outer skin layers).

It is seen in Fig. 11 that maximum D is achieved with c_1 equal to zero; the best beam has a core entirely made of the lower-density foam. Clearly, for optimisation of the stiffness, the benefit of placing dense outer skin material as far as possible from the neutral axis outweighs any benefit brought by reinforcing the core with central or outer regions of higher density. Graded sandwich structures such as those envisaged here, thus, have no practical interest in this sample configuration from the standpoint of flexural rigidity. Note that the present calculations, and hence, the optimum found, differ between the present problem and that treated by Gibson [36].

References

[1] L.J. Gibson, M.F. Ashby, Cellular Solids: Structure and Properties, second ed., Cambridge University Press, Cambridge, UK, 1997, p. 510.
[2] M.F. Ashby, A. Evans, N.A. Fleck, L.J. Gibson, J.W. Hutchinson, H.N.G. Wadley, Metal Foams: A Design Guide, Butterworth Heinemann, Boston, USA, 2000, p. 251.
[3] H.P. Degischer, B. Krizt (Eds.), Handbook of Cellular Metals, Wiley-VCH Verlag, Weinheim, Germany, 2002, p. 373.
[4] J. Banhart, Prog. Mater. Sci. 46 (2001) 559–632.
[5] A.G. Evans, J.W. Hutchinson, M.F. Ashby, Prog. Mater. Sci. 43 (1999) 171–221.
[6] R. Jancek, A. Kottar, H.P. Degischer, in: J. Banhart, N. Fleck, A. Mortensen (Eds.), Proceedings of the Conference Metfoam: 2003, Verlag MIT Publishing, Berlin, Germany, 23–25 June, 2003, pp. 19–24.
[7] A. GrønsundHanssen, M. Langseth, O.S. Hopperstad, Adv. Eng. Mater. 4 (2002) 771–776.
[8] R. Kretz, K. Hausberger, B. Götzinger, Adv. Eng. Mater. 4 (2002) 781–785.
[9] H.W. Seeliger, in: J. Banhart, N. Fleck, A. Mortensen (Eds.), Proceedings of the Conference Metfoam: 2003, Verlag MIT Publishing, Berlin, Germany, 23–25 June, 2003, pp. 5–12.
[10] C. Chen, A.-M. Harte, N. Fleck, Int. J. Mech. Sci. 43 (2001) 1483–1506.
[11] C. Chen, N.A. Fleck, M.F. Ashby, Adv. Eng. Mater. 4 (2002) 777–780.
[12] A.M. Harte, N.A. Fleck, M.F. Ashby, Int. J. Fatigue 23 (2001) 499–507.
[13] O. Kesler, L.J. Gibson, Mater. Sci. Eng. A236 (2002) 228–234.
[14] T.M. McCormack, R. Miller, O. Kesler, L.J. Gibson, Int. J. Solids Struct. 38 (2001) 4901–4920.
[15] O. Kesler, L.K. Crews, L.J. Gibson, Mater. Sci. Eng. A341 (2003) 264–272.
[16] A.M. Harte, N.A. Fleck, M.F. Ashby, Adv. Eng. Mater. 2 (2000) 219–222.
[17] H. Bart-Smith, J.W. Hutchinson, A.G. Evans, Int. J. Mech. Sci. 43 (2001) 1945–1963.
[18] H. Bart-Smith, J.W. Hutchinson, N.A. Fleck, A.G. Evans, Int. J. Solids Struct. 39 (2002) 4999–5012.
[19] T. Beck, D. Löfe, F. Baumgärtner, Adv. Eng. Mater. 4 (2002) 787–790.
[20] C. Körner, M. Hirschmann, M. Lamm, R.F. Singer, in: J. Banhart, N. Fleck, A. Mortensen (Eds.), Proceedings of the Conference Metfoam: 2003, Verlag MIT Publishing, Berlin, Germany, 23–25 June, 2003, pp. 209–214.
[21] F.W. Bach, D. Bormann, P. Wilk, in: J. Banhart, N. Fleck, A. Mortensen (Eds.), Proceedings of the Conference Metfoam: 2003, Verlag MIT Publishing, Berlin, Germany, 23–25 June, 2003, pp. 215–218.
[22] F. Baumgärtner, I. Duarte, J. Banhart, Adv. Eng. Mater. 2 (2000) 168–174.
[23] R. Kretz, E. Wolfsgruber, in: J. Banhart, N. Fleck, A. Mortensen (Eds.), Proceedings of the Conference Metfoam: 2003, Verlag MIT Publishing, Berlin, Germany, 23–25 June, 2003, pp. 181–186.
[24] M. Brunnbauer, C. Körner, R.F. Singer, in: J. Banhart, N. Fleck, A. Mortensen (Eds.), Proceedings of the Conference Metfoam: 2003, Verlag MIT Publishing, Berlin, Germany, 23–25 June, 2003, pp. 187–190.
[25] C. Chen, N.A. Fleck, J. Mech. Phys. Solids 50 (2002) 955–977.
[26] P. Onck, E.W. Andrews, L.J. Gibson, Int. J. Mech. Sci. 43 (2001) 681–699.
[27] E.W. Andrews, G. Gioux, P. Onck, L.J. Gibson, Int. J. Mech. Sci. 43 (2001) 701–713.
[28] T. Daxner, F.G. Rammerstorfer, H.J. Bohm, Mater. Sci. Tech. Ser. 16 (2000) 935–939.
[29] S. Suresh, A. Mortensen, Fundamentals of Functionally Graded Materials, The Institute of Materials, London, UK, 1998, p. 165 (Book 698).
[30] C. SanMarchi, J.F. Despois, A. Mortensen, Acta Mater. 52 (2004) 2895–2902.
[31] C.W. SanMarchi, A. Mortensen, in: H.P. Degischer, B. Kriszt (Eds.), Handbook of Cellular Metals, Wiley-VCH Verlag, Weinheim, Germany, 2002, pp. 43–56.
[32] C. Gaillard, J.F. Despois, A. Mortensen, Mater. Sci. Eng. A 374 (2004) 250–262.

[33] C. SanMarchi, A. Mortensen, Acta Mater. 49 (2001) 3959–3969.

[34] J.F. Despois, Y. Conde, C.S. Marchi, A. Mortensen, in: J. Banhart, N. Fleck, A. Mortensen (Eds.), Proceedings of the Conference Metfoam: 2003, Verlag MIT Publishing, Berlin, Germany, 23–25 June, 2003, pp. 375–380.

[35] H.G. Allen, Analysis and Design of Structural Sandwich Panels, Pergamon Press, Oxford, UK, 1969, p. 283.

[36] L.J. Gibson, Mater. Sci. Eng. 67 (1984) 125–135.

[37] V.S. Deshpande, N.A. Fleck, J. Mech. Phys. Solids 48 (2000) 1253–1283.